Journal Name



ARTICLE TYPE

Cite this: DOI: 10.1039/xxxxxxxxxx

Electron Dynamics in MoS₂-Graphite Heterostructures

Xinwu Zhang,^a Dawei He,^a Lixin Yi,*^a Siqi Zhao,^a Jiaqi He,^a Yongsheng Wang,*^a and Hui Zhao,^b

Received Date Accepted Date

DOI: 10.1039/xxxxxxxxxx

www.rsc.org/journalname

The electron dynamics in heterostructures formed by multilayer graphite and monolayer or bulk MoS_2 were studied by femtosecond transient absorption measurements. Samples of monolayer MoS_2 -multilayer graphite and bulk MoS_2 -multilayer graphite were fabricated by exfoliation and a dry transfer techniques. Ultrafast laser pulses were used to inject electron-hole pairs in monolayer or bulk MoS_2 . The transfer of these photocarriers to the adjacent multilayer graphite was time resolved by measuring the differential reflection of a probe pulse. We found that photocarriers injected in monolayer MoS_2 transfer to graphite on an ultrafast time scale shorter than 400 fs. Such an efficient charge transfer is key to developing high performance optoelectronic devices with MoS_2 as the light absorbing layer and graphite as electrodes. The absorption coefficient of monolayer MoS_2 can be controlled by the carriers in graphite. This process can be used for interlayer coupling and control. In the bulk MoS_2 -graphite heterostructure, the photocarrier transfer time is about 220 ps, due to the inefficient interlayer charge transport in bulk MoS_2 . These results provide useful information for developing optoelectronic devices based on MoS_2 -graphite heterostructures.

1 Introduction

Stimulated by the discovery of graphene, a single layer of carbon atoms with a hexagonal lattice, in 2004¹, studies of materials composed of single layers of atoms or molecules, known as two-dimensional (2D) materials, have increased dramatically ^{2–4}. So far, hundreds of 2D materials have been investigated, including elementary materials such as phosphorene, antimonene, silicine, and germanene, as well as compounds of transition metal dichalcogenides (TMDs), transition metal oxides, and hexagonal boron nitride. These materials have shown various promising properties for a broad range of applications.

One of the most intriguing aspects of 2D materials is the possibility of combining two or more different 2D layers to form new multilayer materials, the so-called van der Waals heterostructures⁵. The van der Waals nature of the interlayer coupling allows for the arbitrary selection of partnering materials, without the lattice-matching constrain. This makes it possible to design and construct new multilayer materials that combines the advantages

Graohene and MoS2 are two of the most extensively studied 2D materials. Naturally, their heterostructures have been a representative system in this field and have attracted much attention. Indeed, combining graphene or graphite and MoS2 is highly relevant for optoelectronic applications. Graphene and graphite have exceptional charge transport performance⁶, while MoS₂ has high absorbance in visible range⁷. Hence, one could use MoS₂ as the light absorbing or emission layer and graphite as the electrodes for various optoelectronic devices. By now, significant progress has been made in developing photodetectors 8-10 and photovoltaic devices 11,12. Furthermore, field-effect transistors ^{13–16}, memory devices ¹⁷, and vertical tunneling transistors ¹⁸ based on this material were reported. Low resistance contact between graphene electrode and MoS₂ has been achieved ^{19,20}. Additionally, application of MoS2-graphene heterostructures in plasmonics 21 and detection of DNA hybridization 22 were explored. For most research, the samples were obtained by manually stacking MoS₂ and graphene layers together ^{23,24}. However, various techniques for scalable growth of MoS2-graphene heterostructures have also been developed ^{25–27}.

One key issue determining the performance of optoelectronic devices based on MoS₂-graphene heterostructures is efficient transfer of photoexcited electrons and holes from MoS₂ to graphene. However, so far, this process has been rarely studied in

of its component layers, for a targeted application.

^a Key laboratory of Luminescence and Optical Information, Ministry of education, Institute of Optoelectronic Technology, Beijing Jiaotong University, Beijing 100044, China

^b Department of Physics and Astronomy, The University of Kansas, Lawrence, Kansas 66045

[†] Electronic Supplementary Information (ESI) available: Characterization of samples; experimental setup; See DOI: 10.1039/b000000x/

a time-resolved fashion. In most heterostructures formed by two TMD monolayers, the band alignments are type-II, where the conduction band minimum and valence band maximum are in separate layers. Transient absorption measurements have revealed ultrafast charge separation and interlayer exciton formation in most systems studied $^{28-34}$. However, since the minima of the conduction and valance bands of graphite are located in the forbidden band of most TMDs 35,36 , both electrons and holes excited in TMD layer are expected to transfer to graphite. Previously, some of us, with other co-workers, have shown that photocarriers injected in monolayer WS₂ can efficiently transfer to monolayer graphene 37 .

Here we report a comprehensive study on the dynamics of electrons and holes in heterostructures formed by multilayer graphite and monolayer and bulk MoS₂ flakes. We found that electrons and holes injected in monolayer MoS₂ transfer to multilayer graphite on a time scale shorter than several hundred femtoseconds. We also found that population of carriers in graphite can effectively change the absorption of MoS₂ monolayer, which can be utilized for interlayer coupling and control of such heterostructures. In the heterostructure formed by a bulk-like MoS₂ flake and multilayer graphite, photocarriers excited in MoS₂ transfer to graphite on a much longer time scale of about 220 ps, which can be attributed to the longer distance the photocarriers has to travel. This study provides important information on developing MoS₂-graphite heterostructures for optoelectronic applications.

2 Experimental section

The heterostructure samples were fabricated by standard exfoliation and a dry transfer process 12 . MoS_2 flakes were first exfoliated from a bulk crystal onto polydimethylsiloxane (PDMS) substrates using adhesive tapes. A flake containing a large monolayer region and a uniform bulk-like region was selected to form heterostructures, and was transferred to a Si-SiO $_2$ substrate.

The thickness of the monolayer region was confirmed by photoluminescence, Raman spectroscopy, and atomic force microscopy (see ESI Fig. S1 and S2). The bulk-like region has a thickness of about 27 nm, according to atomic force microscopy (see ESI Fig. S2), and hence contains about 40 layers. Next, a thin graphite flake was prepared with the same technique. Atomic force microscopy measurement shows a thickness of about 5 nm (see ESI Fig. S2), corresponding to about 14 layers. The graphite flake was transferred to MoS₂, such that both the monolayer and the bulk-like regions are partially covered (see ESI Fig. S1). Therefore, the sample contains monolayer MoS₂, monolayer MoS₂graphite, bulk MoS₂, and bulk MoS₂-graphite regions, to facilitate their direct comparison. The sample was annealed under a Ar environment at a base pressure of about 5 Torr at 200°C for 4 hours.

The electron dynamics were studied by transient absorption measurements in reflection geometry ³⁸. The experimental scheme is shown in ESI (Fig. S3). A Ti-doped sapphire laser generates 100-fs and 820-nm pulses at about 80 MHz. Part of the beam is used to pump an optical parametric oscillator to generate an output that is tunable around 670 nm, which serves as the probe beam for the measurements. The other part of the 820-nm beam is focused to a beta barium borate (BBO) crystal to gen-

erate its second harmonic at 410 nm. Depending on the sample and configurations, either the 410- or the 820-nm beam was used as the pump. Beamsplitters were used to combine the pump and probe beams and to send both into a microscope objective lens, which focused both to the sample surface with spot size of about 1 μ m. Part of the probe beam that is reflected by the sample was sent to a silicon photodiode. A lock-in amplifier was used to measure the voltage output of the photodiode, which is proportional to the probe power, and hence provides a measurement of the reflectance of the sample at the probe photon energy.

By using a spinning-wheel chopper, the pump intensity reaching the sample was modulated between a set value and zero at about 2 KHz. This causes the photodiode output to alternate, at the same frequency, between two values corresponding to the reflectance of the sample with and without the presence of the pump beam, respectively. The amplitude of this alternative signal was detected by using a lock-in amplifier that was synchronized at the chopping frequency. With this configuration, we obtain the differential reflection, which is defined as the pump-induced relative change of the reflectance, $\Delta R/R_0 = (R-R_0)/R_0$, where *R* and R_0 are the probe reflectance with and without the presence of the pump, respectively. In most measurements, this quantity was recorded as a function of the probe delay, which is defined as the arrival time of the probe pulse with respect to the pump pulse. All the measurements were performed at room temperature with the sample exposed to air. No sample degradation was observed during the entire study.

3 Results and discussion

3.1 Monolayer MoS₂

To better understand the electron dynamics in heterostructures formed by monolayer MoS2 and graphite, we first studied the monolayer MoS₂ region of the sample. Figure 1(a) shows the pump-probe scheme. A pump pulse of 100 fs and 3.02 eV (blue arrow) excites electron-hole pairs (circles). The differential reflection of a probe pulse of 100 fs and 1.85 eV was detected to monitor these photocarriers. Figure 1(b) and (c) show the signal measured with a pump fluence of about 1 μ J cm⁻², on short and long time ranges, respectively. The rising of the signal is limited by the time resolution of the measurement, indicating that the excited electron-hole pairs can instantaneously induced transient absorption at the A-exciton resonance of MoS_2^{39} . This is consistent with previously reported ultrafast thermalization and cooling of photocarriers in atomically thin MoS₂ ⁴⁰. The fast (subpicosecond) drop of the signal right after zero probe delay can be attributed to exciton formation 41. The rest of the decay can be fit by a biexponential function, with two time constants of 14 \pm 2 and 150 \pm 20 ps, respectively. Previously, multiple exponential decay process of transient absorption signal has been generally observed in TMD monolayers ^{42,43}. The longer time constant can be attributed to the exciton lifetime.

The measurement was repeated with different values of the pump fluence. The decay of the signal was found to be independent of the fluence, while the change of the peak signal with the pump fluence is shown in Figure 1(d). The dependence can be

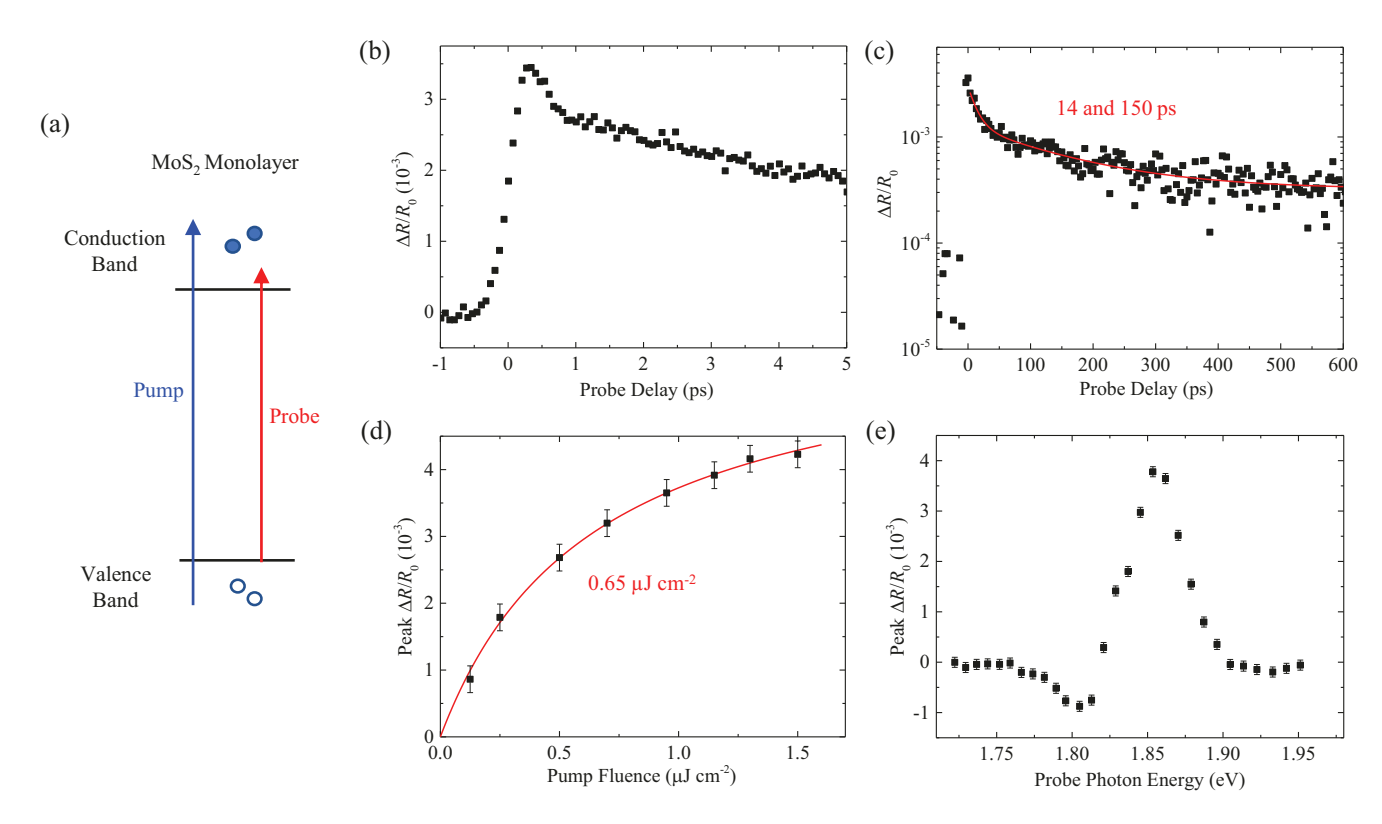


Fig. 1 (a) Pump-probe scheme used to study a monolayer MoS_2 sample, showing the pump (blue) exciting electron-hole pairs (circles), which are monitored by the probe (red). (b) Differential reflection signal measured from a monolayer MoS_2 sample with 3.02 eV and 1 μ J cm⁻² pump and 1.85 eV probe. (c) Same as (b) but over a larger time range. (d) Peak differential reflection signal as a function of the pump fluence. The red curve shows a fit to the data. (e) Peak differential reflection signal as a function of the probe photon energy.

fit by a saturated absorption model, $\Delta R/R_0 = AF/(F+F_s)$, where A is a dimensionless constant, F the pump fluence, and F_s , the saturation fluence 38 . The red curve in Figure 1(d) corresponds to a saturation fluence of 0.65 μ J cm $^{-2}$. We also repeated the measurement with different values of probe photon energy. The results are shown in Figure 1(e). Both positive (photobleaching) and negative (photoinduced absorption) signals were observed around the A-exciton resonance, which is consistent with previous studies 38 . Despite of the complicated mechanism involved in the carrier-induced transient absorption process, the results confirms that the 1.85 eV probe used in (b), (c), and (d) indeed senses the change of the excitonic resonance of MoS₂.

3.2 Monolayer MoS₂-graphite heterostructure

Next, we studied monolayer MoS₂-graphite heterostructure under the same experimental conditions. It has been shown that the minima of the conduction and valence bands of graphite are located in the forbidden band of monolayer MoS₂⁴⁴. Hence, as illustrated in Figure 2(a), the pump-injected electron-hole pairs are expected to transfer to the graphite layer (orange arrow). The same 1.85 eV probe was used to monitor the exciton resonance of MoS₂. The blue symbols in Figure 2 summarize the results in a similar fashion as Figure 1. Comparing the two figures, we found that in the heterostructure sample the signal is larger by about a factor of 10 and the signal decays single-exponentially with a time constant of about 10 ps, which is much faster than the 150-

ps lifetime of excitons in monolayer MoS_2 . The magnitude of the signal is proportional to the pump fluence, as shown in Figure 2(d), and thus is proportional to the injected carrier density.

In the following, we argue that the enhanced and fast-decaying signal originates from photocarriers that are excited in MoS₂ and then subsequently transfer to graphite. To establish this, we first ruled out the transient absorption from the graphite layer as the origin of the enhanced signal by measuring the signal as a function of the probe photon energy. As shown in Figure 2(e), the magnitude of the signal depends strongly on the probe photon energy, and drops to about zero when tuned away from the exciton resonance of MoS₂. This result shows that the signal is dominated by the change of the absorption of the MoS₂ layer, instead of the graphite layer. Indeed, previous studies 45,46 have shown that transient absorption signal from graphite with pump fluences on the order of 1 μJ cm $^{-2}$ is on the order of 10^{-5} , which is much smaller than the signal observed here.

Since the signal originates from the absorption change of MoS_2 exciton resonance induced by the pump-injected carriers, the 10-fold enhancement would not have been observed if the carriers injected in MoS_2 remain in that layer. When populating MoS_2 , they do not yield such a large transient absorption, as shown in Figure 1. One reasonable interpretation is that these carriers transfer to graphite after their injection. Once in graphite, they produce a larger transient absorption at the exciton resonance of MoS_2 .

Generally speaking, the presence of electron-hole pairs or ex-

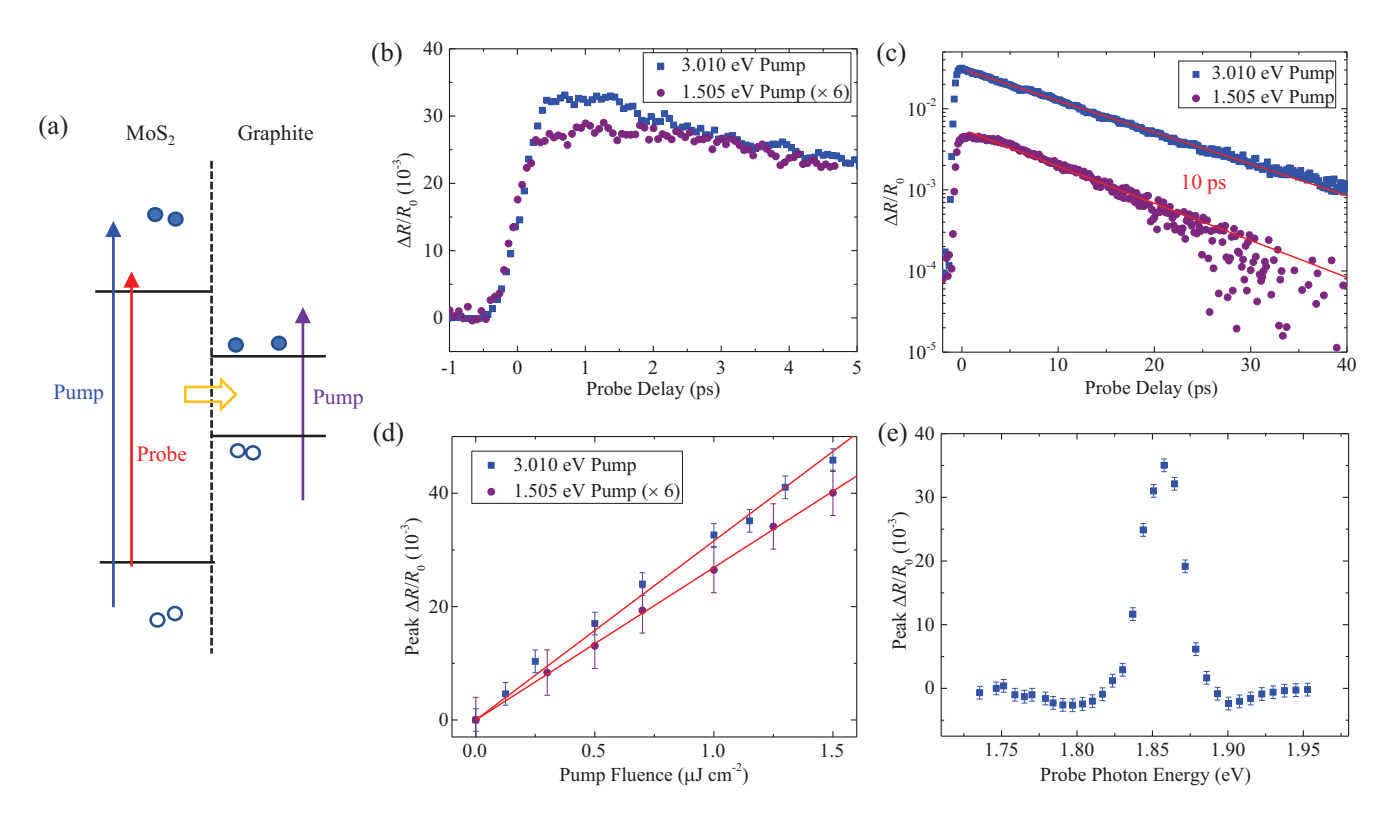


Fig. 2 (a) Pump-probe scheme used to study a monolayer MoS_2 -graphite heterostructure sample, showing the pump (blue) exciting electron-hole pairs (circles) that transfer to graphite (orange arrow). (b) Differential reflection signal measured with 3.010 (blue) and 1.505 eV (purple) pumps, respectively, and 1.85 eV probe. (c) Same as (b) but over a larger time range. The red line is an exponential fit. (d) Peak differential reflection signal as a function of the fluence of the 3.010 eV (blue) and 1.505 eV (purple) pumps. The red lines show linear fits to the data. (e) Peak differential reflection signal as a function of the probe photon energy for the 3.010 eV pump.

citons can induce a change of the absorption around exciton resonance, that is, transient absorption, *via* phase-space filling and bandgap renormalization ⁴⁷. In 2D materials, due to the enhanced Coulomb interaction between the electrons and the holes, it can be expected that screening of this interaction by photocarriers can play an important role in inducing transient absorption. Since a significant portion of the electric field lines between electrons and holes extend beyond the 2D layer, the carriers in an adjacent layer can effectively alter the electron-hole interaction by screening effect, and thus inducing transient absorption of the layer that they do not populate. Due to the smaller effective mass and the higher mobility of carriers in graphite, it is reasonable that the screening effect is larger for carriers in graphite than in MoS₂.

The above hypothesis can be tested by selectively injecting carriers in the graphite layer only, by using a pump photon energy that is smaller than the optical bandgap of MoS_2 , as shown by the purple arrow in Figure 2(a). Since MoS_2 is not excited and the carriers excited in graphite do not have enough energy to transfer to MoS_2 , no carrier population is expected in the MoS_2 layer. Hence, any transient absorption signal would be due to carriers in the graphite layer. The purple symbols in Figure 2 show the results of such a measurement, with a pump photon energy of 1.505 eV. A signal was indeed detected, with similar time and pump fluence dependences as the 3.010 eV pump. The signal is about 6

times weaker than the 3.010 eV pump under the same conditions, which can be attributed to the smaller absorbance of the sample at 1.505 eV due to the lack of absorption by MoS_2 . Finally, since both curves shown in Figure 2(b) have similar rising times, we can conclude that the transfer of electron-hole pairs from MoS_2 to graphite occurs on a time scale shorter than the time-resolution of the measurement, which is about 400 fs. The 10-ps decay of the signal can then be attributed to the lifetime of electron-hole pairs in graphite, which is also consistent with previous reports for multilayer graphite 48,49 .

3.3 Bulk MoS₂-graphite heterostructure

Finally, we studied the heterostructure formed by the bulk-like region of MoS $_2$ flake and graphite. First, pump-probe measurements were performed on the region of the flake that was not covered by graphite. The experimental procedures and conditions are the same as those used to study the monolayer MoS $_2$ region. The first row of Figure 3 summarizes the results. Similar to the monolayer sample, the signal reaches a peak rapidly [Figure 3(a)]. The decay of the signal is much slower than monolayer. A single exponential fit [red curve in (b)] yielded a decay time constant of about 1 ns, which shows the extended photocarrier lifetime in bulk MoS $_2$ ⁵⁰. Pump-fluence dependence shown in Figure 3(c) corresponds to a saturation fluence of 6 \pm 1 μ J cm $^{-2}$, which is much larger than the monolayer sample. The magnitude

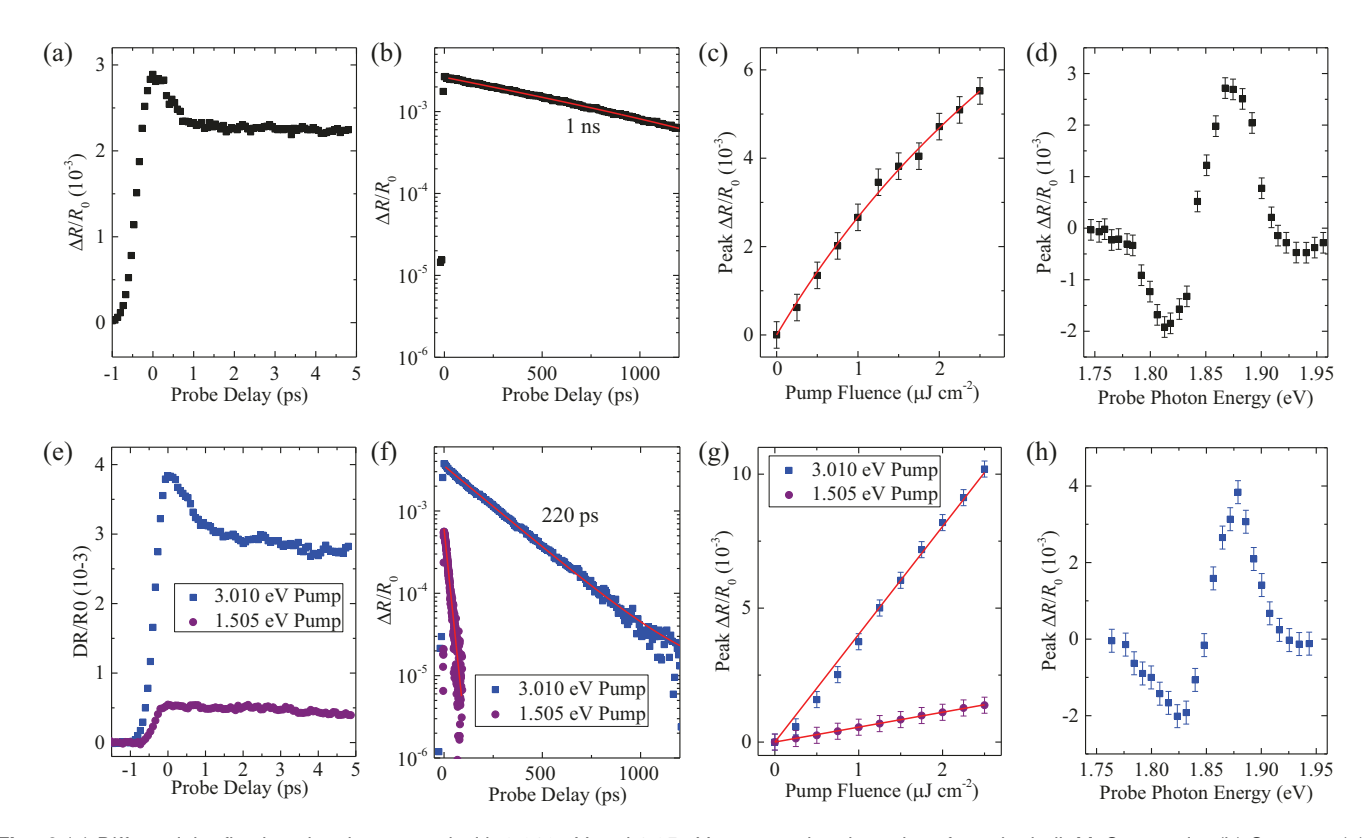


Fig. 3 (a) Differential reflection signal measured with 3.010 eV and 1.85 eV pump and probe pulses from the bulk MoS_2 sample. (b) Same as (a) but over a larger time range. The red line is an exponential fit with a time constant of 1 ns. (c) Peak differential reflection signal as a function of the pump fluence. (d) Peak differential reflection signal as a function of the probe photon energy. (e) - (h) are the same as (a) - (d), but for the bulk MoS_2 -graphite heterostructure. Blue and purple symbols are for the 3.010 and 1.505 eV pumps, respectively.

of the signal shows a derivative-like dependence on the probe photon energy near the exciton resonance, indicating the dominant role of the shifting of the resonance by carriers ³⁸.

The blue symbols in the bottom row of Figure 3 show the results of the same measurement performed with the region of the bulk-like MoS₂ flake that is covered by graphite. The signal is slightly larger, by about 30 %, in the heterostructure. Hence, the graphite layer still enhanced the signal, but compared to the heterostructure formed by monolayer MoS₂ and graphite, the effect is much smaller. This can be attributed to the larger thickness of the MoS₂ layer: For most layers of MoS₂, the graphite layer is further away and hence the screening effect is smaller. As shown in Figure 3(f), the signal in bulk MoS₂-graphite heterostructure decays faster, with a time constant of about 220 ps. The signal is proportional to the pump fluence (g) and shows similar dependence on the probe photon energy (h).

To interpret these features, we first establish that the differential reflection of this sample mostly monitors the population of the photocarriers in MoS_2 , instead of graphite as in the monolayer heterostructure. Otherwise, the signal would decay with a 10-ps time constant - the lifetime of carriers in graphite - instead of 220 ps. This is further supported by the fact that the signal is only slightly larger in the heterostructure than bulk MoS_2 . The decay of the signal thus reflects the decrease of the photocarrier density in MoS_2 . Since the photocarrier lifetime in bulk MoS_2 was measured to be 1 ns, the faster decay can only be attributed to the

transfer of carriers from bulk MoS_2 to graphite. The much slower transfer can be understood as the consequence of the longer distance an average carrier must travel due to the increased thickness of MoS_2 . To test these interpretations, we changed the pump photon energy to 1.505 eV and repeated the measurements. The purple symbols in the bottom row of Figure 3 summarize the results. The signal is about 6 times smaller than the 3.010 eV pump, due to the smaller absorption of MoS_2 . The decay of the signal is graphite-like, with a time constant of about 10 ps.

4 Conclusion

We have time resolved, for the first time, electron dynamics in heterostructures formed by multilayer graphite and monolayer or bulk MoS_2 . We found that photocarriers injected in monolayer MoS_2 transfer to multilayer graphite on an ultrafast time scale shorter than 400 fs. Such an efficient charge transfer shield light on the mechanism of high performance optoelectronic devices with MoS_2 as light absorbing layer and graphite as electrodes. We also found that the absorption coefficient of MoS_2 can be manipulated by carriers in graphite - a process that can be utilized to achieve interlayer coupling and control. In heterostructures formed by bulk MoS_2 and graphite, the charge transfer time is about 220 ps, due to the inefficient interlayer charge transport in bulk MoS_2 . These results provide useful information for developing high performance optoelectronic devices based on MoS_2 -graphite heterostructures.

Acknowledgement

We are grateful for the financial support of the National Key R&D Program of China(2016YFA0202302), the National Natural Science Fund Project of China (61335006,61527817,61275058,61378073), the Initiative Postdocs Supporting Program (BX201600013), and the National Science Foundation of USA (DMR-1505852).

References

- 1 K. S. Novoselov, A. K. Geim, S. V. Morozov, D. Jiang, Y. Zhang, S. V. Dubonos, I. V. Grigorieva and A. A. Firsov, *Science*, 2004, **306**, 666–669.
- 2 A. Allain, J. H. Kang, K. Banerjee and A. Kis, *Nat. Mater.*, 2015, **14**, 1195–1205.
- 3 A. D. Franklin, Science, 2015, 349, 704.
- 4 L. Zhong, M. Amber, B. Natalie, S. Shruti, Z. Kehao, S. Yifan, L. Xufan, J. B. Nicholas, Y. Hongtao, K. F.-S. Susan, C. Alexey, Z. Hui, M. Stephen, M. L. Aaron, X. Kai, J. L. Brian, D. Marija, C. M. H. James, P. Jiwoong, C. Manish, E. S. Raymond, J. Ali, C. H. Mark, R. Joshua and T. Mauricio, *2D Mater.*, 2016, 3, 042001.
- 5 A. K. Geim and I. V. Grigorieva, *Nature*, 2013, **499**, 419–425.
- 6 S. V. Morozov, K. S. Novoselov, M. I. Katsnelson, F. Schedin, D. C. Elias, J. A. Jaszczak and A. K. Geim, *Phys. Rev. Lett.*, 2008, **100**, 016602.
- 7 H.-L. Liu, C.-C. Shen, S.-H. Su, C.-L. Hsu, M.-Y. Li and L.-J. Li, Appl. Phys. Lett., 2014, 105, 201905.
- 8 W. J. Yu, Y. Liu, H. Zhou, A. Yin, Z. Li, Y. Huang and X. Duan, *Nat. Nanotechnol.*, 2013, **8**, 952–958.
- 9 D. D. Fazio, I. Goykhman, D. Yoon, M. Bruna, A. Eiden, S. Milana, U. Sassi, M. Barbone, D. Dumcenco, K. Marinov, A. Kis and A. C. Ferrari, *ACS Nano*, 2016, **10**, 8252–8262.
- 10 W. J. Yu, Q. A. Vu, H. Oh, H. G. Nam, H. L. Zhou, S. Cha, J. Y. Kim, A. Carvalho, M. Jeong, H. Choi, A. H. C. Neto, Y. H. Lee and X. F. Duan, *Nat. Commun.*, 2016, 7, 13278.
- 11 M. Shanmugam, R. Jacobs-Gedrim, E. S. Song and B. Yu, *Nanoscale*, 2014, **6**, 12682–12689.
- 12 L. Britnell, R. M. Ribeiro, A. Eckmann, R. Jalil, B. D. Belle, A. Mishchenko, Y.-J. Kim, R. V. Gorbachev, T. Georgiou, S. V. Morozov, A. N. Grigorenko, A. K. Geim, C. Casiraghi, A. H. C. Neto and K. S. Novoselov, *Science*, 2013, 340, 1311–1314.
- 13 W. J. Yu, Z. Li, H. L. Zhou, Y. Chen, Y. Wang, Y. Huang and X. F. Duan, *Nat. Mater.*, 2013, **12**, 246–252.
- 14 L. Britnell, R. V. Gorbachev, R. Jalil, B. D. Belle, F. Schedin, A. Mishchenko, T. Georgiou, M. I. Katsnelson, L. Eaves, S. V. Morozov, N. M. R. Peres, J. Leist, A. K. Geim, K. S. Novoselov and L. A. Ponomarenko, *Science*, 2012, 335, 947–950.
- C. J. Shih, Q. H. Wang, Y. Son, Z. Jin, D. Blankschtein and M. S. Strano, ACS Nano, 2014, 8, 5790–5798.
- J. Y. Kwak, J. Hwang, B. Calderon, H. Alsalman, N. Munoz,
 B. Schutter and M. G. Spencer, *Nano Lett.*, 2014, 14, 4511–4516.
- 17 K. Roy, M. Padmanabhan, S. Goswami, T. P. Sai, G. Ramalingam, S. Raghavan and A. Ghosh, *Nat. Nanotechnol.*, 2013,

- 8, 826-830.
- 18 Y. Sata, R. Moriya, S. Morikawa, N. Yabuki, S. Masubuchi and T. Machida, *Appl. Phys. Lett.*, 2015, **107**, 023109.
- 19 Y. Liu, H. Wu, H. C. Cheng, S. Yang, E. B. Zhu, Q. Y. He, M. N. Ding, D. H. Li, J. Guo, N. O. Weiss, Y. Huang and X. F. Duan, *Nano Lett.*, 2015, 15, 3030–3034.
- 20 D. Qu, X. Liu, F. Ahmed, D. Lee and W. J. Yoo, *Nanoscale*, 2015, **7**, 19273–19281.
- 21 R. N. Liu, B. X. Liao, X. D. Guo, D. B. Hu, H. Hu, L. J. Du, H. Yu, G. Y. Zhang, X. X. Yang and Q. Dai, *Nanoscale*, 2017, 9, 208–215.
- 22 P. T. Loan, W. Zhang, C. T. Lin, K. H. Wei, L. J. Li and C. H. Chen, *Adv. Mater.*, 2014, **26**, 4838–44.
- 23 H. C. Diaz, R. Addou and M. Batzill, Nanoscale, 2014, 6, 1071.
- 24 Y. F. Lin, W. W. Li, S. L. Li, Y. Xu, A. Aparecido-Ferreira, K. Komatsu, H. B. Sun, S. Nakaharai and K. Tsukagoshi, *Nanoscale*, 2014, **6**, 795–799.
- 25 M. V. Zhao, Y. Ye, Y. M. Han, Y. Xia, H. Y. Zhu, S. Q. Wang, Y. Wang, D. A. Muller and X. Zhang, *Nat. Nanotechnol.*, 2016, 11, 954–959.
- 26 D. McManus, S. Vranic, F. Withers, V. Sanchez-Romaguera, M. Macucci, H. F. Yang, R. Sorrentino, K. Parvez, S. K. Son, G. Iannaccone, K. Kostarelos, G. Fiori and C. Casiraghi, *Nat. Nanotechnol.*, 2017, 12, 343–350.
- 27 X. Chen, Y. J. Park, T. Das, H. Jang, J. B. Lee and J. H. Ahn, *Nanoscale*, 2016, **8**, 15181–15188.
- 28 X. Hong, J. Kim, S. F. Shi, Y. Zhang, C. Jin, Y. Sun, S. Tongay, J. Wu, Y. Zhang and F. Wang, Nat. Nanotechnol., 2014, 9, 682–686.
- 29 F. Ceballos, M. Z. Bellus, H. Y. Chiu and H. Zhao, *ACS Nano*, 2014, **8**, 12717–12724.
- 30 M. Z. Bellus, F. Ceballos, H.-Y. Chiu and H. Zhao, *ACS Nano*, 2015, **9**, 6459–6464.
- 31 K. Wang, B. Huang, M. Tian, F. Ceballos, M.-W. Lin, M. Mahjouri-Samani, A. Boulesbaa, A. A. Puretzky, C. M. Rouleau, M. Yoon, H. Zhao, K. Xiao, G. Duscher and D. B. Geohegan, *ACS Nano*, 2016, **10**, 6612–6622.
- 32 B. Peng, G. Yu, X. Liu, B. Liu, X. Liang, L. Bi, L. Deng, T. C. Sum and K. P. Loh, *2D Mater.*, 2016, **3**, 025020.
- 33 S. D. Pan, F. Ceballos, M. Z. Bellus, P. Zereshki and H. Zhao, *2D Mater.*, 2017, **4**, 015033.
- 34 F. Ceballos, M. G. Ju, S. D. Lane, X. C. Zeng and H. Zhao, *Nano Lett.*, 2017, **17**, 1623–1628.
- 35 Y. Z. Guo and J. Robertson, *Appl. Phys. Lett.*, 2016, **108**, 233104.
- 36 Y.-J. Yu, Y. Zhao, S. Ryu, L. E. Brus, K. S. Kim and P. Kim, *Nano Lett.*, 2009, **9**, 3430–3434.
- 37 J. He, N. Kumar, M. Z. Bellus, H. Y. Chiu, D. He, Y. Wang and H. Zhao, *Nat. Commun.*, 2014, **5**, 5622.
- 38 F. Ceballos and H. Zhao, *Adv. Funct. Mater.*, 2017, **27**, 1604509.
- 39 R. Wang, B. A. Ruzicka, N. Kumar, M. Z. Bellus, H.-Y. Chiu and H. Zhao, *Phys. Rev. B*, 2012, **86**, 045406.
- 40 Z. Nie, R. Long, L. Sun, C. C. Huang, J. Zhang, Q. Xiong,

- D. W. Hewak, Z. Shen, O. V. Prezhdo and Z. H. Loh, *ACS Nano*, 2014, **8**, 10931–10940.
- 41 F. Ceballos, Q. Cui, M. Z. Bellus and H. Zhao, *Nanoscale*, 2016, **8**, 11681–11688.
- 42 H. Shi, R. Yan, S. Bertolazzi, J. Brivio, B. Gao, A. Kis, D. Jena, H. G. Xing and L. Huang, *ACS Nano*, 2012, 7, 1072–1080.
- 43 T. Yan, X. Qiao, X. Liu, P. Tan and X. Zhang, *Appl. Phys. Lett.*, 2014, **105**, 101901.
- 44 D. Pierucci, H. Henck, J. Avila, A. Balan, C. H. Naylor, G. Patriarche, Y. J. Dappe, M. G. Silly, F. Sirotti, A. T. C. Johnson, M. C. Asensio and A. Ouerghi, *Nano Lett.*, 2016, 16, 4054–4061.

- 45 B. A. Ruzicka, L. K. Werake, H. Zhao, S. Wang and K. P. Loh, *Appl. Phys. Lett.*, 2010, **96**, 173106.
- 46 B. A. Ruzicka and H. Zhao, Phys. Rev. B, 2009, 79, 155204.
- 47 S. Schmitt-Rink, D. S. Chemla and D. A. B. Miller, *Phys. Rev. B*, 1985, **32**, 6601–6609.
- 48 P. A. George, J. Strait, J. Dawlaty, S. Shivaraman, M. Chandrashekhar, F. Rana and M. G. Spencer, *Nano Lett.*, 2008, **8**, 4248.
- 49 D. Sun, C. Divin, C. Berger, W. A. de Heer, P. N. First and T. B. Norris, *Phys. Rev. Lett.*, 2010, **104**, 136802.
- 50 N. Kumar, J. He, D. He, Y. Wang and H. Zhao, *J. of Appl. Phys.*, 2013, **113**, 133702.